Learning from Nature to Improve the Heat Generation of Iron-Oxide Nanoparticles for Magnetic Hyperthermia Applications

Carlos Martinez-Boubeta[1,], Konstantinos Simeonidis[2], Antonios Makridis[3], Makis Angelakeris[3], Oscar Iglesias[4], Pablo Guardia[5], Andreu Cabot[1,5], Lluis Yedra[1], Sonia Estradé[1,6], Francesca Peiró[1], Zineb Saghi[7], Paul A. Midgley[7], Iván Conde-Leborán[8], David Serantes[8] & Daniel Baldomir[8]*

[1]*Departament d'Electrònica and IN2UB, Universitat de Barcelona, Martí i Franquès 1, 08028 Barcelona, Spain.*

[2]*Department of Mechanical Engineering, University of Thessaly, 38334 Volos, Greece*

[3]*Department of Physics, Aristotle University of Thessaloniki, 54124 Thessaloniki, Greece*

[4]*Departament de Física Fonamental and Institute IN2UB, Universitat de Barcelona, Av. Diagonal 647, 08028 Barcelona, Spain*

[5]*IREC, Jardins de les Dones de Negre 1, 08930 Sant Adrià del Besòs, Spain.*

[6]*TEM-MAT, CCiT-Universitat de Barcelona, Solé i Sabaris 1, 08028 Barcelona, Spain.*

[7]*Department of Materials Science and Metallurgy, University of Cambridge, Pembroke Street, Cambridge CB2 3QZ, United Kingdom.*

[8]*Instituto de Investigacións Tecnolóxicas, and Departamento de Física Aplicada, Universidade de Santiago de Compostela, 15782 Santiago de Compostela, Spain.*

ADDITIONAL INFORMATION

MICROSCOPY CHARACTERIZATION

Figure S1. TEM image of the 20 nm spherical nanoparticles.

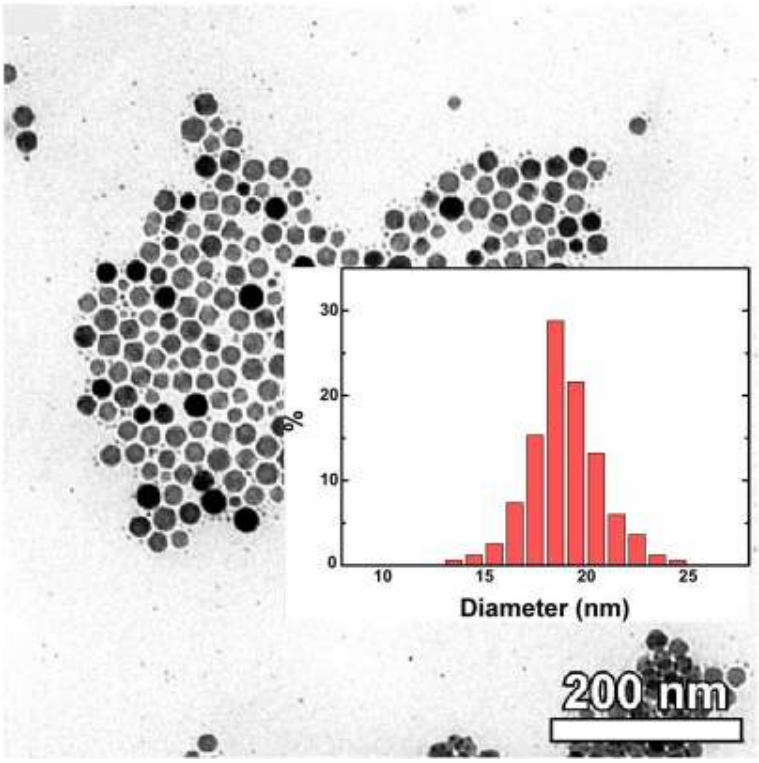

TOMOGRAPHIC RECONSTRUCTION

Tomographic reconstruction is achieved using a tilt series covering a range of -64º ≤ α ≤ 64º at an increment of 4º in a FEI Tecnai F20-G2 FEGTEM (200kV). In order to fulfill the projection requirement (Hawkes, P.W. The electron microscope as a structure projector, in: J. Frank (Ed.), Electron Tomography, 2nd ed. Springer-Verlag, **2006,** 83-111), the signal acquired was the high angle annular dark field (HAADF) as the contrast of these images is only proportional to the thickness and the atomic number of the samples. The reconstruction method was the Simultaneous Iterative Reconstruction Technique (SIRT, Gilbert, P. *J. Theor. Biol.* **1972,** *36,* 105-117) with 40 iterations. The reconstructed volume was afterwards manually segmented in order to minimize the elongation effects of the missing wedge of tilt angles.

Movie S1. (attached) A movie clip is included in order to visualize the reconstruction and three-dimensional structure.

Figure S2 presents snapshots of the tomographic recording (on the left) and direct visualization of the reconstruction of the agglomerate volume before segmentation (on the right). From the reconstructed and segmented 3D volume, one particle highlighted in blue was carved out (see Fig. 2 within the main paper). We stress that it is energetically favorable for the (truncated) nanocubes, like in our case, to orient in the face-face configuration due to the {100} facets.

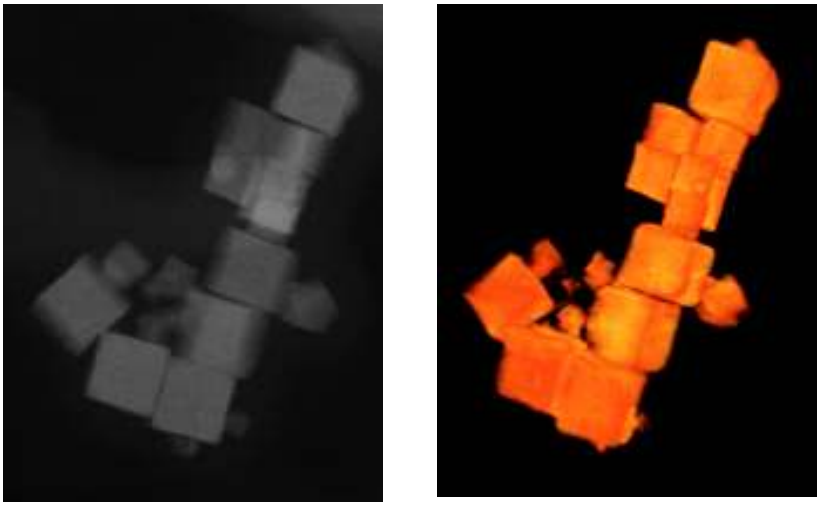

DYNAMIC LIGHT SCATTERING CHARACTERIZATION

Figure S3. Dynamic light scattering experiments of the colloidal solution displaying the hydrodynamic diameter of the aggregates. Results suggest that cuboids self aggregate in aqueous solution, the average number of particles per chain is roughly 7-10. On the other hand, spherical nanoparticles show mean value 34 ± 9 nm, slightly larger than the sizes observed in the TEM images.

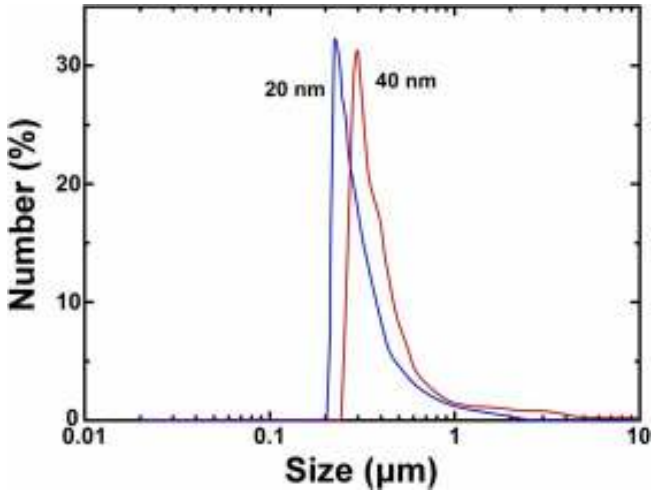

THERMOGRAVIMETRIC ANALYSIS

Figure S4. TGA patterns. A first weight loss of 1-2 %wt. corresponding to moisture occurs below 200 ºC while the gradual decomposition of the bound surfactant molecules takes place between 300-500 ºC. In this range weight decreases about 5 %wt. for 20 nm cuboids and 3 %wt. for 40 nm ones. The theoretical calculation results a percentage of 4.7 and 2.7 respectively for the two samples. The spherical nanoparticles appear to have excess surfactants. On further heating (500-700 ºC range), a lower weight loss is also observed, which could be possibly due to the removal of oxygen atoms from the ferrite lattice by residual carbon [Ayyappan, S. *et al. Mater. Chem. Phys.* **2011,** *130,* 1300].

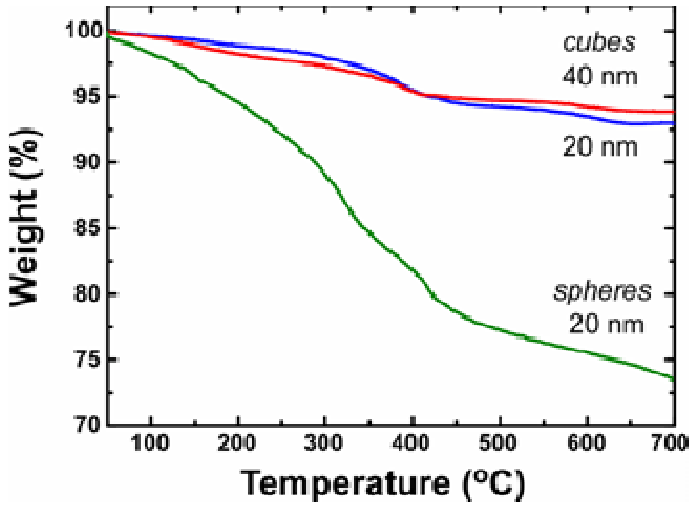

MAGNETIC CHARACTERIZATION

Figure S5. Hysteresis loops of 20 nm spherical nanoparticles.

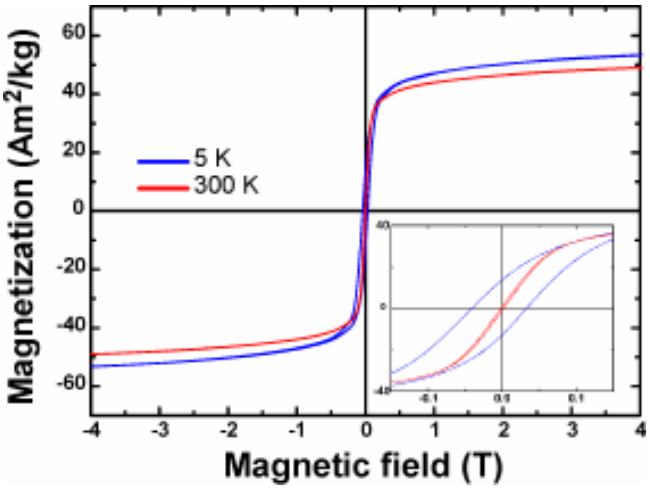

Figure S6. Temperature dependence of the magnetization of the iron oxide samples under ZFC and FC conditions. Our previous measurements showed the nanoparticles structure is based on Fe_3O_4, but with cation vacancies on decreasing the particle size [Martínez-Boubeta, C. *et al. Phys. Rev. B* **2006,** *74,* 054430]. Accordingly, the 40 nm cubes show incontrovertible evidence for magnetite: the sharp drop in ZFC and FC magnetization near the Verwey transition temperature (T_V ~ 120 K), denoted by arrow. Noteworthy, the ZFC curve exhibits a pronounced increase upon heating. Though, above T_V the ZFC and FC curves for the 40 nm sample are similar. Differences arise from the fact the magnetocrystalline anisotropy constant (K_1) goes through zero. Thus, from now on, we surmise the 40 nm cuboids are mainly composed of Fe_3O_4 while the 20 nm sample resembles maghemite.

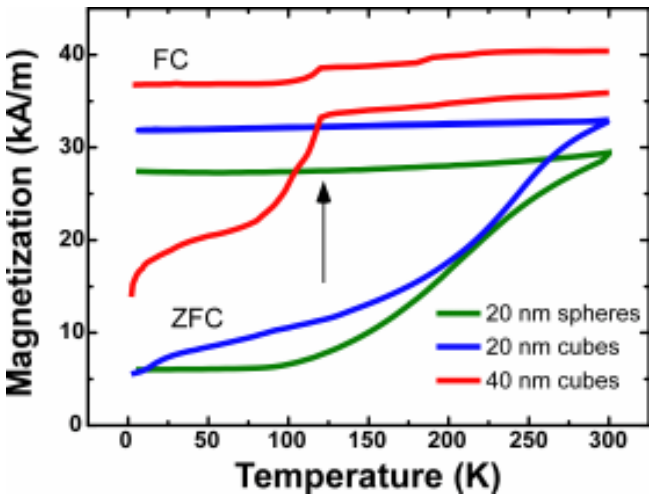

HYPERTHERMIA MEASUREMENTS

Figure S7. Experimental heating curves, from room temperature, at different iron oxide concentrations. (a-c) 20 nm nanocubes with concentrations ranging from 0.5 mg down to 2 mg of iron oxide per ml, at a frequency of 765 kHz and several magnetic field amplitudes: 15 mT (red line), 20 mT (blue line), 25 mT (black line) and 30 mT (green line). (d-f) Temperature evolution as a function of time for 40 nm cuboids measured under the same experimental conditions as those used in (a-c).

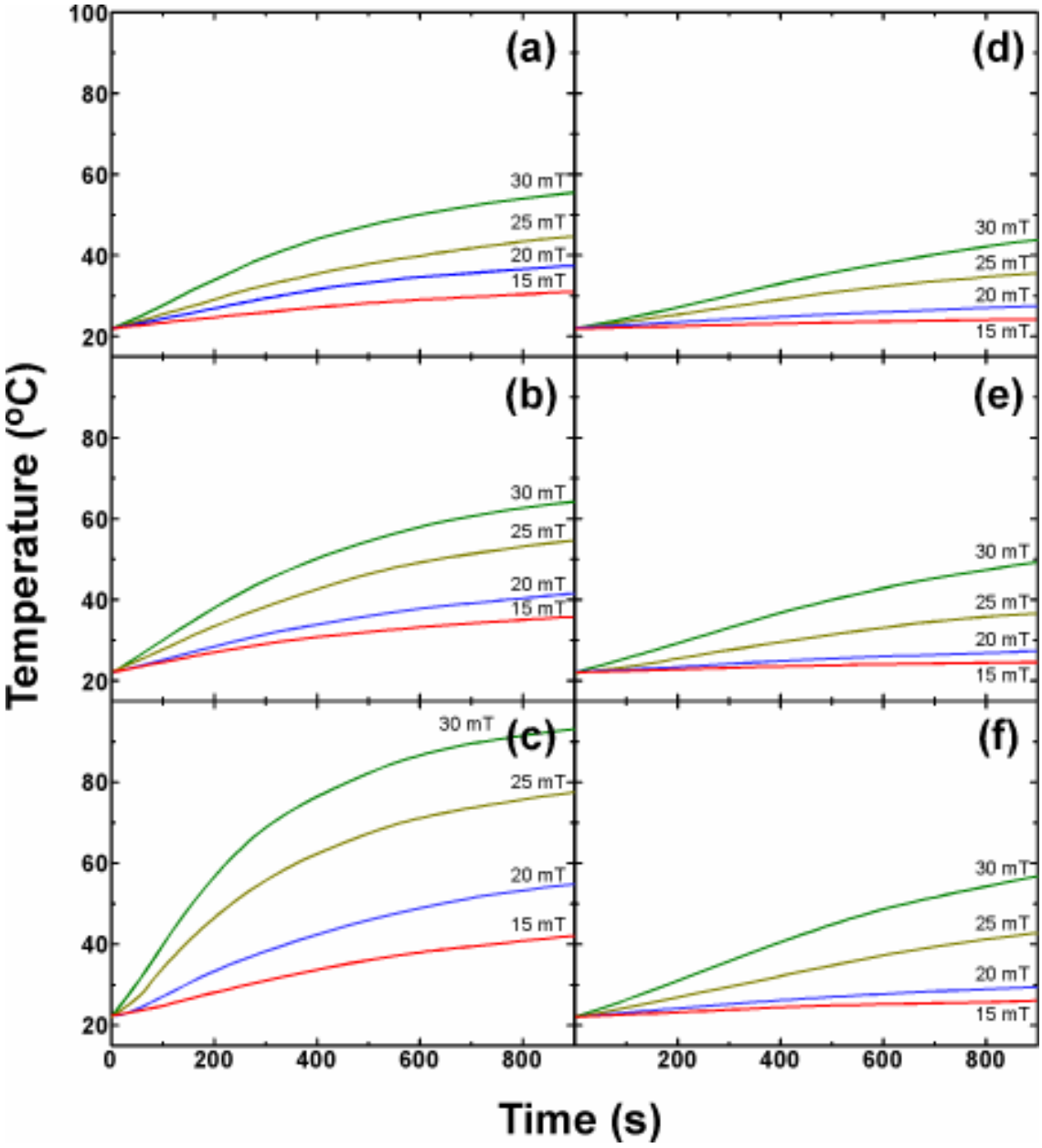

For a safe application of hyperthermia to patients, it was suggested that the product of the frequency and the magnetic field amplitude should be smaller than 5×10^8A/ms (Hergt, R.; Dutz, S. *J. Magn. Magn. Mater.* **2007,** *311,*187). Additionally, a nice survey of literature from January 1990 to October 2010, regarding glioma in vitro studies and assays using animals, can be found in Silva *et al. Int. J. Nanomedicine.* **2011,** *6,* 591. It is observed that the oscillation frequency of the magnetic field, collected for all studies, is mainly defined as being close to 100 kHz. This is also the frequency in use for the first human trials by the company MagForce AG (see for instance Maier-Hauff, *et al. J. Neurooncol.* **2011,** *103,* 317). Yet noteworthy are the first clinical trials ever reported by Gilchrist *et al.* (*Annals of Surgery.* **1957,** *146,* 596), where a frequency of 1.2 MHz and field intensities up to about 300 Oe were used.

While it is admitted that a time-varying magnetic field can cause unpleasant peripheral nerve stimulation when the maximum excursion of the magnetic field is above a frequency-dependent threshold level, please note the aforementioned $H_{max}f$ factor was derived from experiments where 'test person had a sensation of warmth, but was able to withstand the treatment for more than one hour without major discomfort' at low frequency hyperthermia. Obviously, in dependence on the seriousness of the illness this critical $H_{max}f$ product may be exceeded in clinic. For instance, since the eddy current power density is proportional to the square of the diameter of the induced current loops, this criterion would be accordingly weaker for smaller body regions being under field exposure; a combination of field amplitude of about 10 kA/m and frequency of about 400 kHz was suggested for the treatment of breast cancer (Hilger, *et al. J. Magn. Magn. Mater.* **2005,** *293,* 314). In this regard, a very recent study suggests the possibility of new designs for human and preclinical systems, since the degree of unpleasant sensation with magnetic fields up to 0.4 T is shown to decrease significantly above 100 kHz (Weinberg *et al.* **2012,** *Med Phys. 39,* 2578).

On the other hand, please note most importantly clinic applications up-to-date deal with huge amounts of iron oxide nanopowders (see for instance Maier-Hauff *et al. J. Neurooncol.* **2011,** *103,* 317) and may contain concentrations as much as 4 M Fe. In doing so, an uniform heating of the tumour can be obtained even by using low intensity, low frequency fields and non-optimized nanoparticles (see figure below). Though, the possible toxicity and side-effects of this approach need to be explored fully.

Figure S8 shows that it is possible to obtain the desired temperature increase for hyperthermia therapy even by using non-optimized particles, if present in sufficiently high concentrations. Though, please note the calculated SAR is very low (1 W/g). Again, this is an effect of dipolar interactions that need to be considered when designing real clinic protocols.

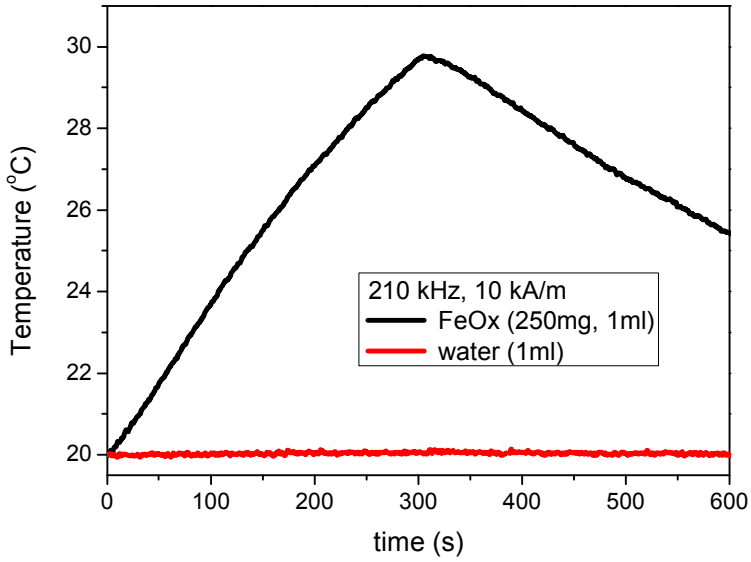

DETERMINATION OF THE EFFECTIVE MAGNETIC ANISOTROPY CONSTANT

The temperature dependences of magnetic parameters, such as the coercive field, are interpreted in terms of the changes in the magnetic anisotropy. The reader should please note the values of the magnetocrystalline anisotropy reported in the literature differ considerably; see for instance Abbasi *et al. J. Phys. Chem. C* ***2011,*** *115,* 6257. Additionally, the effective anisotropy can be larger than the bulk magnetocrystalline anisotropy. For instance, Lartigue *et al. J. Am. Chem. Soc.* **2011***, 133,* 10459 have found decreasing values of K_{eff} on increasing size.

We estimated the effective magnetic anisotropy in the iron oxide particles from the experimental data using the law of approach to magnetic saturation. The high field magnetization curves can be analyzed, at sufficiently high fields, in terms of the law of approach to saturation (see, for instance, Brown, W. F. Jr. Theory of the approach to magnetic saturation. *Phys. Rev.* **1940,** *58,* 736)

$$M = M_S(1 - b/H^2) \quad (1)$$

where M_S is the saturation magnetization and b is correlated with the effect of the magnetocrystalline anisotropy. Thus, by knowing the fitting parameter b the anisotropy constant can be calculated as $K_{eff} = \mu_0 M_S(15b/4)^{1/2}$ in the case of uniaxial magnetic crystals. The fitting parameters are given below (Table S1). Discrepancies, as it turns out, can be attributed to dipolar coupling between particles (please see also Table S2)

Table S1.

Fitting parameters		20 nm cube	40nm cube	20nm sphere
5K	M_S [kA m^{-1}]	440	505	370
	K_{eff} [kJ m^{-3}]	98	54	15
300K	M_S [kA m^{-1}]	385	465	340
	K_{eff} [kJ m^{-3}]	77	42	12

Importantly, we surmise cubic particles exhibit higher anisotropy energy values than that for spheres due to surface contribution. For the cubic nanoparticles, values are higher than those for bulk Fe_3O_4 (about 11 kJ m^{-3}) or γ-Fe_2O_3 (13 kJ m^{-3}) at room temperature and were found to increase with decreasing nanoparticle size. Noteworthy, a similar trend was recently observed by Zhen *et al. J. Phys. Chem. C* **2011,** *115,* 327, but quite the reverse of what Salazar-Alvarez *et al. J. Am. Chem. Soc.* **2008,** *130*, 13234 reported. Those different results could be a consequence of differences in the chemical composition of the nanoparticles with dissimilar sizes and morphology, as already pointed by Chalasani *et al. J. Phys. Chem. C* **2011,** *115,* 18088. In this regard, the presence of core/shell structures within a single particle modifies K_{eff} (see for instance, Shavel *et al. Adv. Func. Mater.* **2007,** *17,* 3870). Nonetheless, in our case since the nanoparticles do not show exchange-bias effects (already reported in Guardia *et al. J. Phys. Chem. C* **2011,** *115,* 390) a homogeneous oxide composition is anticipated. This was further supported by high-resolution TEM (see Fig. 1).

SIMULATION DETAILS

We present numerical Monte Carlo calculations using the Metropolis algorithm to simulate the magnetization of interacting ferromagnetic nanoparticles. It is assumed that the nanoparticles are monodomain, with the magnetization change taking place by coherent rotation of the atomic magnetic moments, which means the spin canting effect at the particle surface is not considered. The anisotropy of the particles is of uniaxial type originated from the crystalline contribution, which dominates over the cubic symmetry. First, easy axes directions were distributed at random, as discussed in detail elsewhere (Serantes *et al. J. Appl. Phys.* **2010,** 108, 073918). For each simulation all particles characteristics (magnetic moment, anisotropy, size), are equal, so that we eliminate polydispersity effects in our results. Also, their positions are kept fixed, thus resembling a frozen ferrofluid (reasonable approximation for the particles even inside the cells during hyperthermia treatment). Regarding the computational procedure, the hysteresis losses were determined in the quasistatic limit. Before we proceed we call attention to the fact the frequency and damping parameters have been shown to produce only small alterations to simulation results [Haase, C. & Nowak, U. Role of dipole-dipole interactions for hyperthermia heating of magnetic nanoparticle ensembles. *Phys. Rev. B* **2012,** *85,* 045435].

We used a large system of N = 1000 particles with periodic boundary conditions. In order to estimate the heating power of the system, we simulated M(H) curves with a 10 Oe field variation every 1000 Monte Carlo steps. This field-variation ratio was chosen so that Stoner-Wohlfarth characteristics (coercive field $H_C \approx 0.5H_A$ and remanence $M_R \approx 0.5M_S$) are approximately reproduced at very low temperatures for all particle types, under the conditions of non-interaction and maximum applied field larger than the anisotropy field of the particles. The fitting parameters M_S and volume used for the calculations were independently extracted from the experimental data. Iron oxide density was taken as 5200 kg m^{-3}. Regarding K, the exact value of the anisotropy constant is not known for most experimental conditions. Another unknown factor is the possibility of a surface anisotropy in the experimental particles and the effect of the interparticle interactions. Thus, to include the effects of concentration, K_{eff} is adjusted so that the calculated hysteresis curves best fit the experimental SQUID data. The parameters considered accounting for the different types of particles are summarized in Table S2.

Table S2. K_{eff} values used in calculations.

Simulation parameters		20 nm cube	40 nm cube	20 nm sphere
5 K	K_{eff} [kJ m^{-3}]	26.9	14.7	--
300 K	K_{eff} [kJ m^{-3}]	3.8	2.6	3.0

Three main aspects are to be investigated: first, the influence of interparticle dipolar interactions on the hyperthermia output of the system, which experimentally are observed to diminish the SAR (see Fig. 4 within the manuscript); second, the observed growing dependence of the SAR on the maximum applied field value (see Figures 4 and 5); and third, the higher hyperthermia output of the 20 nm cubic particles in comparison with the spherical particles of the same volume ($d \approx 25$ nm). Our results indicate that, i) the absolute values of K are much smaller than the effective ones estimated from the experiment; ii) the cubic particles have a higher anisotropy, as foreseen from the experimental data and predicted by the atomistic MC simulations (see Fig. 5 and Figure S11); iii) magnetic dipolar interactions decrease the SAR for both the cubic and

spherical particles; iv), the SAR grows with H_{max}, for the different fields considered. It is remarkable that the experimental trends of the features described above are clearly reproduced, supporting the feasibility of our simulations to study hyperthermia properties.

Figure S9. Simulated M(H) curves corresponding to Fig. 4 within the main manuscript. Inset: detail of the coercive fields.

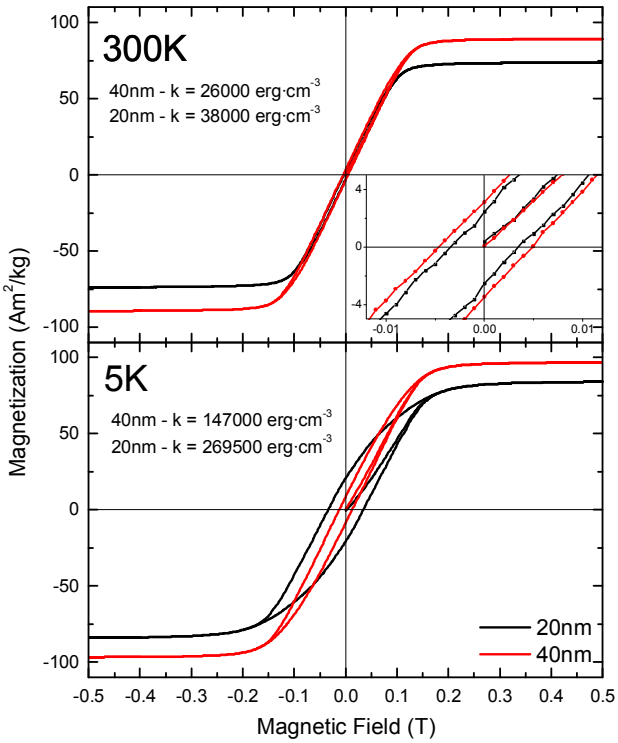

Importantly, data suggest the 20 nm particles at room temperature are in the transition regime between superparamagnetism and a blocked state. In principle this would indicate a lower hyperthermia performance in comparison with particles in the blocked state, for which the hysteresis losses are much more relevant. However, it is worth to note that since the hyperthermia measurements are performed at a much higher frequency ($f \sim 10^5$ Hz), the particle moments will be in that case well below the superparamagnetic transition, ensuring large hysteresis losses. Obviously, the available field-intensities probe only losses from minor hysteresis loops for the 40 nm sample, thus explaining the smaller SAR values compared to the 20 nm case.

At this point it is very important to note that although the simulated values correspond to the energy dissipated in one cycle, it is possible to make a give a good estimation (see Fig. S10) of the results in W/g units, obtaining values very close to the experimental ones. Therefore, to estimate the SAR from the simulations in frequency units, one only has to multiply the hysteresis losses of one cycle times *f*.

Figure S10. Calculated area enclosed by hysteresis loops for the 20 nm nanocubes and its concentration dependence.

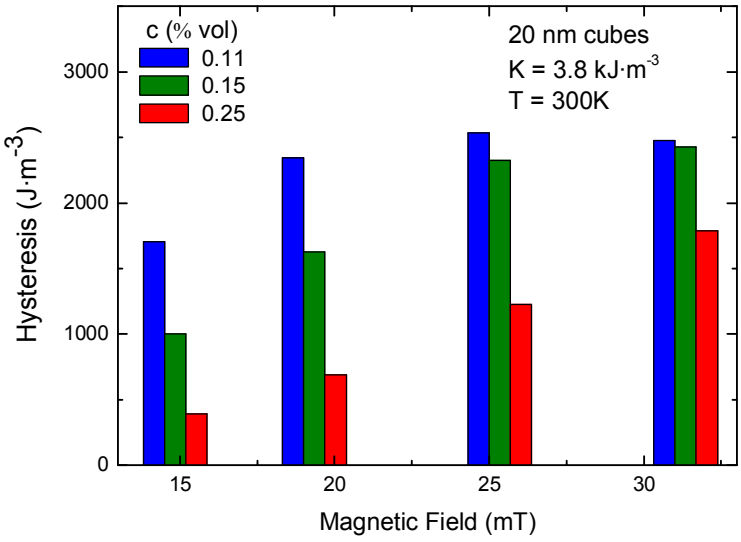

On the other hand, it is well know that a more or less uniformly magnetized state prevails for small spherical nanoparticles. This also remains true for magnetic nanocubes in spite of the divergence of the stray field at the edges and corners (see below). Simulations of individual spherical and cubic nanoparticles were performed on the basis of a system of classical Heisenberg spins by using the Monte Carlo method with the standard Metropolis algorithm. The spins are placed in the positions of the Fe ions of the real maghemite structure as done also in Iglesias, O. & Labarta, A. *Phys. Rev. B* **2001,** *63,* 184416 and then the particles are built by cutting the lattice in a spherical shape or a cube with rounded corners with the same dimensions as in the real samples (12 unit cells diameter/cube length). To compute the energy changes during the simulation, we considered the following Hamiltonian:

$$H / k_B = -\sum_{\langle i,j \rangle} J_{ij} \left(\vec{S}_i \cdot \vec{S}_j \right) - \sum_i \vec{h} \cdot \vec{S}_i + E_{anis} \qquad (2)$$

$$E_{anis} = -k_S \sum_{i \in S} \sum_{j \in nn} \left(\vec{S}_i \cdot \hat{r}_{ij} \right)^2 - k_C \sum_{i \in C} \left(\vec{S}_i \cdot \hat{n}_i \right)^2$$

where the first term accounts for the nn exchange interactions with Jij set to reported values for maghemite, the second is the Zeeman energy with $h = \mu H / k_B$ (H is the magnetic field and μ the magnetic moment of the magnetic ion). The anisotropy energy term E_{anis} distinguishes two kinds of contributions: Néel type anisotropy for the spins with reduced coordination with respect to bulk (surface S spins) and uniaxial anisotropy along the magnetic field direction for the core (C) spins. The standard bulk value is used for $k_C = 4.7 \times 10^5$ J/m^3 which translates into a reduced approximate value of $k_C = 0.01$ K/spin. Surface anisotropy constant values were chosen as $k_S = 10$ K for the spherical particle and $k_S = 30$ K for the cubic one, so as to reproduce the effective anisotropies deduced from the experiments. These value were computed by using the well-known relation between anisotropies $k_{eff} = k_C + S/V\ k_S$ (where S and V are the surface and volume of the nanoparticle). Compared with spherical particles we can see both the coercivity and area of the hysteresis loops of cuboids increased (see Fig. S11), so the increased hysteresis losses may give rise to the enhanced heating capacity. For the spherical particle, the smoothness of central area of the loop indicates a quasi-coherent magnetization reversal (as corroborated also by detailed inspection of the snapshots in Fig. S12) with the surface spins progressively aligning towards the field direction as the magnetic field is increased beyond the closure field of the loop. In contrast, the loop of the cubic particle displays a kink-like feature for fields slightly above the coercive fields and presents much higher closure fields. Inspection of the Fig. S11 reveals that the origin of these differential features is in the contribution of surface spins of the lateral faces of the cube that have local anisotropy axis pointing close to the direction perpendicular to the field. Consequently, the peculiar geometry and increased anisotropy of cubic particles translate into an enhanced contribution of surface spins to the coercive and closure fields, producing at the same time non-uniform spin structures during magnetization reversal even below the supposed single domain limit.

Figure S11. Contribution of the surface spins only to the hysteresis loop of a spherical (red circles) and a cubic particle with the same characteristics as those in Figure 6.

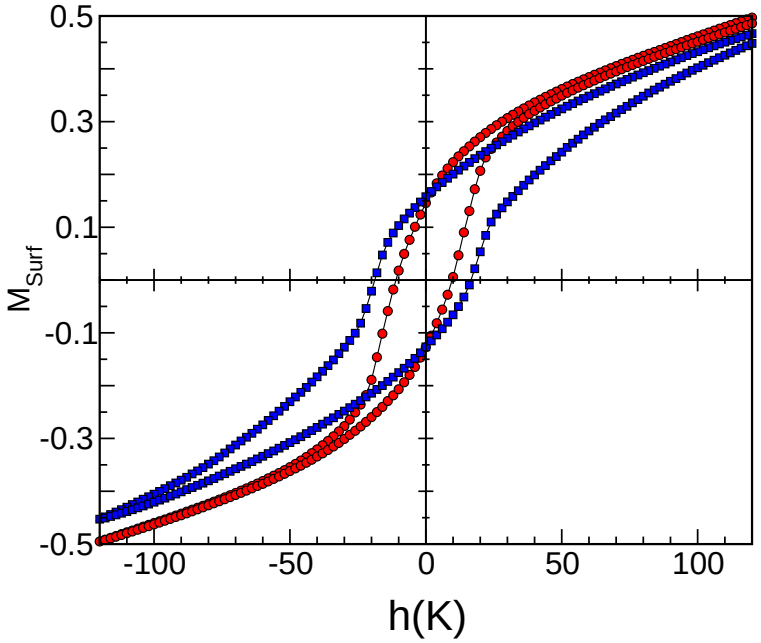

Figure S12 (on the next page) shows snapshots of the spin configurations at representative points of the hysteresis loops shown in Fig. 6 as indicated: M_{rem}^{+} (M_{rem}^{-}), remanent state at the descreasing (increasing) field branch; H_C^{+} (H_C^{-}), near the positive (negative) coercive field. Spins have been colored according to their projection into the magnetic field direction (z axis) from red (+1) to blue (-1).

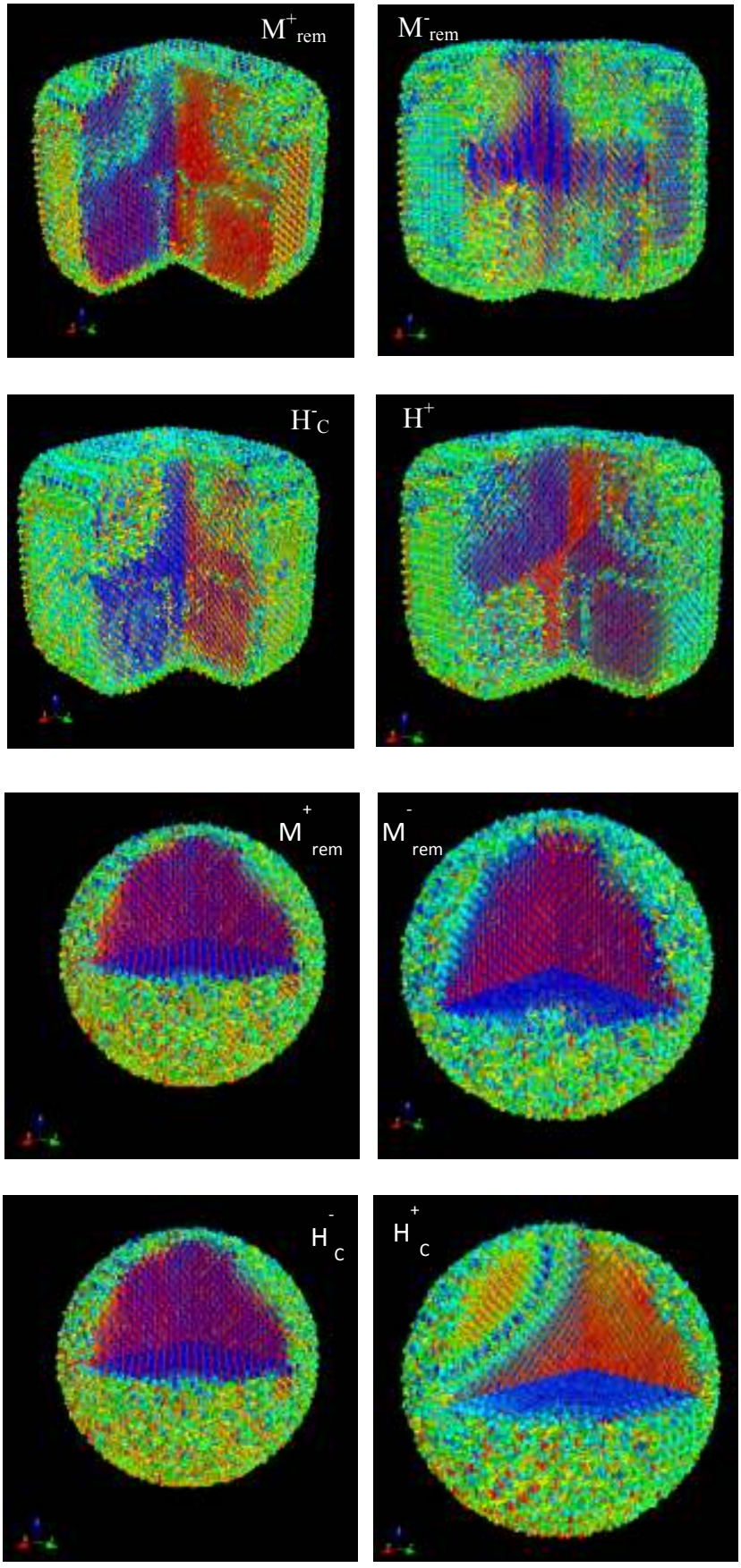
M^{+}_{rem}
M^{-}_{rem}
H^{-}_{C}
H^{+}
M^{+}_{rem}
M^{-}_{rem}
H^{-}_{C}
H^{+}_{C}